 ©2025 Uspekhi Fizicheskikh Nauk, Russian Academy of Sciences

*CONFERENCES AND SYMPOSIA*

PACS numbers: **07.57. – c,** 74.81.Fa, 85.25.Cp

# Superconducting terahertz generators *

F.V. Khan, L.V. Filippenko, A.B. Ermakov, M.E. Paramonov, M.Yu. Fominsky, N.V. Kinev, V.P. Koshelets, S.A. Nikitov

DOI: https://doi.org/10.3367/UFNe.2024.12.039864

## Contents



**Abstract. Applied devices based on superconducting electronics, due to their quantum nature, unique set of parameters, and cryogenic operating temperatures, are significantly superior to systems based on other physical principles. The operating frequency of ultra-sensitive terahertz-range (THz) receivers has reached 1 THz, and their noise temperature is only restricted by the quantum limit. One of the most promising areas is the development of superconducting THz generators for integrated receiver systems. Such an application of the AC Josephson effect seems quite natural; however, many developments and studies conducted in dozens of major laboratories worldwide failed for a long time to create a generator with the required parameters.**

**Keywords:** THz-range Josephson oscillators; high-quality niobium-based tunnel junctions; integrated local oscillators; emission linewidth; frequency and phase stabilization mode

**F.V. Khan** [(a)], **L.V. Filippenko** [(b)], **A.B. Ermakov** [(c)], **M.E. Paramonov** [(d)], **M.Yu. Fominsky** [(e)], **N.V. Kinev** [(f)], **V.P. Koshelets** [(g)], **S.A. Nikitov** [(h)]
Kotelnikov Institute of Radio Engineering and Electronics,
Russian Academy of Sciences,
ul. Mokhovaya 11, korp. 7, 125009 Moscow, Russian Federation
E-mail: [(a)] khanfv@hitech.cplire.ru, [(b)] lyudmila@hitech.cplire.ru,
[(c)] ermakov@hitech.cplire.ru, [(d)] paramonov@hitech.cplire.ru,
[(e)] demiurge@hitech.cplire.ru, [(f)] nickolay@hitech.cplire.ru,
[(g)] valery@hitech.cplire.ru, [(h)] nikitov@cplire.ru

Received 9 December 2024
*Uspekhi Fizicheskikh Nauk* **195** (6) 621 – 634 (2025)
Translated by M.Zh. Shmatikov

## 1. Introduction

Superconducting electronics enable creating devices featuring functionality which is unique compared to conventional approaches, as confirmed by experience throughout the world. Such devices usually operate based on quantum effects, which provide high operating frequencies and maximum efficiency and, in combination with cryogenic temperatures, allow attaining low noise, only limited by quantum values [1–5]. The main incentive for the rapid development of superconducting electronics in recent years has been the possibility of creating devices with record-setting parameters, in demand in various fields of science and technology and operating in a wide frequency range, from fractions of a hertz to X-ray frequencies. Superconducting quantum interference devices (SQUIDs) allow measuring magnetic fields at the level of $10^{-6}$ of magnetic flux quantum $\Phi_0$ [4, 5], while superconducting single-photon detectors (SSPDs) [6–8] make it possible to register single photons with a wavelength of less than 10 μm. Based on SQUIDs, devices have been developed for detecting and processing weak signals, including superconducting parametric amplifiers with a noise temperature below the physical one [9–11] and single-quantum digital devices (Rapid Single Flux Quantum; RSFQ) [12, 13] for interface superconducting circuits that provide communication with quantum bits (qubits) and control of quantum systems at ultra-low temperatures [14, 15].

One of the most successfully developing areas of superconducting electronics is ultrasensitive terahertz (THz)

* This review is based on a report presented at the Scientific Session of the General Meeting of the Physical Sciences Division of the Russian Academy of Sciences on December 9, 2024 (see *Phys. Usp.* **68** 551 (2025); *Usp. Fiz. Nauk* **195** 584 (2025)).

receivers; their operating frequency $f$ has reached 1.2 THz, and the noise temperature is only restricted by the quantum limit or photon noise. To measure the spectral composition of the received radiation, heterodyne receivers with resolution $\Delta f/f$ better than $10^{-6}$ are required. In a heterodyne receiver, the incoming weak input signal is converted (transferred) to a lower intermediate frequency (IF) without phase loss. Mixers based on superconductor-insulator-superconductor (SIS) tunnel junctions [16–19] are the most sensitive input devices in heterodyne receivers; their noise temperature in dual-side band (DSB) mode is limited by the quantum value $hf/(2k_B)$ [20], where $h$ and $k_B$ are the Planck and Boltzmann constants, respectively. The development of heterodyne superconducting receiving systems, including those produced in Russia, has been recently reviewed in *Physics–Uspekhi* [21].

The use of several heterodyne receivers allows the creation of interferometric systems with a high angular resolution, which is determined by the distance between the receiving antennas. It is on this principle that the largest radio astronomy project of our time, the Atacama Large Millimeter/submillimeter Array (ALMA) multi-element interferometer [22], is built, and the Event Horizon Telescope (EHT) program [23] was created, uniting dozens of radio telescopes around the world into a 'single network'. The extremely high angular resolution made it possible to obtain for the first time in history 'image' of a supermassive black hole in the center of the galaxy M 87 [24, 25]. An even higher angular resolution will be implemented in the Russian space agency's Millimetron project to create a space-Earth radio interferometer with a base of up to 1.5 million km [26, 27].

The Millimetron Space Observatory will also study the Universe in the single-telescope mode; it should be noted that the measurements will not be limited by the absorption of Earth's atmosphere in the terahertz frequency range. This circumstance is especially valuable for observing the water molecule, which is essential for the emergence of life, in various space objects (protostellar clouds, protoplanetary disks, and comets) and for identifying patterns in the evolution of water in space. Such measurements will help to answer one of the key questions in modern astrophysics regarding the conditions necessary for the emergence of life. It should be noted that SIS receivers have already successfully operated aboard space observatories, for example, as part of the Herschel Space Observatory program [28, 29].

The local oscillator for terahertz receivers must provide continuous frequency tuning in the entire range of the SIS mixer, sufficient power for its pumping, high spectral ratio (SR), and low phase noise. In addition, especially for space applications, the weight, size, and power consumption of such a heterodyne generator are very important. Currently, most SIS receivers use a complex system of multipliers and power amplifiers as a heterodyne [30, 31], which allows obtaining a power of up to 2 mW at a frequency of 1 THz with 5% efficiency [30]. THz-range heterodynes capable of operating in space telescopes can only be manufactured in a few research centers, one of which is the NASA Jet Propulsion Laboratory (California Institute of Technology) [32]. Therefore, it is fundamentally important for the implementation of the Millimetron space program to develop alternative versions of the local oscillator, one of the most promising options being a superconducting THz-range generator.

The development and exploration of sub-terahertz range generators based on superconducting junctions began with the discovery of the Josephson effect; such an application of the AC Josephson effect seems quite natural. Any Josephson junction is a generator whose frequency is determined by the average voltage across it. Usually, for the convenience of setting the required voltage, junctions with a hysteresis-free current-voltage characteristic (IVC) are used. However, the parameters of a single junction do not allow obtaining sufficiently powerful and narrow-band radiation, so chains and arrays containing tens and hundreds of Josephson junctions were used [33, 34]; a brief overview of generators of this type is presented in Section 2.1.

Until recently, it was possible to implement in one device both terahertz generation with the ability to tune the frequency in a wide range and a narrow emission linewidth required for the practical application of such devices, only for systems based on long Josephson junctions (LJJs) [21, 35, 36]. Section 2.2 overviews early activities on the creation of LJJ generators [37–41] based on conventional superconductors, and Section 2.3, the development of generators based on natural arrays of high temperature superconductors (HTS) Josephson junctions [42–47]. Section 3 presents the results of the development and research of an integrated local oscillator on LJJ current-voltage, obtained at the Kotelnikov Institute of Radioelectronics of the Russian Academy of Sciences in recent years, and Section 4 describes a new type of superconducting generator based on a one-dimensional array of Josephson junctions in a coplanar line.

## 2. Terahertz Josephson generators

### 2.1 Generators based on Josephson junction arrays

Descriptions of various versions of superconducting generators based on Josephson junction arrays, differing in topology, shunting method, and operating frequency range, have been published [33, 34, 48–51]. The junctions can be arranged in a 2D array [51]; such a topology of the structure allows a larger number of junctions to fit on one chip, which, provided they are synchronized, enables achieving higher generation power. If the array has $M$ horizontal columns and $N$ vertical rows, the power is proportional to $\sim MN$, and the generation line $\sim 1/MN$. If the array is one-dimensional, the generation power, provided that the $N$ junctions are synchronized and the matching coefficient with the external load is close to 1, is proportional to $N$. If, however, the array and load are strongly mismatched, the power, according to model [33], increases proportionally to $N^2$. It should be noted that the second option is not suitable for creating a local oscillator in a superconducting receiver, since the output power characteristic as a function of frequency will be strongly nonuniform and will not provide the required level of pumping power to mixer at all frequencies, which will lead to an increase in the noise temperature of the receiver. In addition, in this case, continuous tuning of the generation frequency is not possible.

The junctions in the array can be located either at a distance much smaller than the wavelength $\lambda$ from each other, or at $\lambda/2$. In the latter case, it is easier to achieve synchronization between the junctions in the array, since each junction is located in the antinode of the electromagnetic field of the wave. However, it turns out that, in such a geometry, the generation frequency cannot be tuned over a wide range. If the junctions are located at a small distance from each other, geometric resonances occur at frequencies determined by the length of the entire array. By decreasing the reflection

coefficient from the array edges, the standing wave ratio can be decreased, which enables a smoother tuning of the generation frequency.

Presented below are the results of a study of one-dimensional and two-dimensional arrays of Josephson junctions carried out by various research groups. For example, study [51] reports measurements of a two-dimensional array consisting of $N = 1968$ Josephson junctions located at a distance equal to half the wavelength corresponding to a frequency of 240 GHz. The maximum generation power exceeded 160 μW; this power is already sufficient for application not only on-chip but also for radiation into open space. A two-dimensional array of tunnel Josephson junctions was also investigated in [52], but, in this case, the array was located above a superconducting screen. The authors successfully achieved a power of up to 0.4 μW with an array consisting of 3 rows containing 131 junctions each. The efficiency of converting the input power into radiation was about 30%; the linewidth and generation spectrum were not measured in the studies.

The results of a study of an array consisting of 9996 Nb/NbSi/Nb junctions are presented in [53]; the operating frequencies are in the range from 139 to 343 GHz, with the possibility of continuous frequency tuning. Junctions can be synchronized by exciting modes in the substrate. The generation linewidth at the best points is less than 1 MHz. An array of 11 junctions located at a distance of $\lambda/2$ from each other and shunted by a thin-film resistor was examined in [54]. The authors estimated that the power supplied to the load from the array was 10 μW at a frequency of 625 GHz. The generation linewidth at this point, determined from the spectrum at the intermediate frequency, was 8 MHz. The authors also succeeded in obtaining a signal from the array at frequencies above the niobium band gap frequency (700 GHz). However, the generation region only consisted of individual frequency points.

Terahertz generators based on arrays of lumped Josephson junctions are currently being developed by many research groups. The main goal of the studies is to enhance the generation power, expand the operating band, and provide synchronization between the junctions in the array.

### 2.2 Long Josephson junctions

The distributed Josephson tunnel junction is one of the most studied types of Josephson generators: It is a long tunnel SIS junction with overlapping geometry [1–3, 37–41, 55–58]. The junction length $L$ is greater than its width $W$ and is many times greater than the Josephson penetration depth of the magnetic field $\lambda_J$. The operating principle of the LJJ generator is as follows. A constant bias current $I_{bias}$ is set across the junction and an external magnetic field (parallel to the junction plane) is applied, which is regulated by the current $I_{CL}$ through the control line.

The magnetic field impacts the penetration of magnetic flux quanta into the junction at one of its edges, altering the Josephson phase $\varphi(x)$ and forming a vortex containing a magnetic flux quantum $\Phi_0$. The bias current drives this quantum, creating a unidirectional flow of Josephson vortices in the junction. The in-plane length and $2\lambda_L$ in the direction perpendicular to the junction plane, where $\lambda_L$ is the London depth of field penetration into the junction (a typical value of $\lambda_L$ for niobium films is 90 nm). Driven by the Lorentz force, fluxons repel each other and form a chain of vortices, which becomes quite rigid in strong magnetic fields [55, 56]. When a moving fluxon crosses the opposite edge of the junction, a voltage pulse occurs, the integral of which over time is equal to the value of the 'emitted' quantum of magnetic flux:

$$\int V\,\mathrm{d}t = \Phi_0 = 2\ \mathrm{mV} \times 1\ \mathrm{ps}\,. \tag{1}$$

The frequency of the emitted signal is related to the voltage $V_{DC}$ at the LJJ by the fundamental Josephson relation $f = (2\pi/\Phi_0)V_{DC}$; thus, at a voltage at the junction of 1 mV, the radiation frequency is 483.6 GHz. The speed and density of the fluxon chain can be controlled by changing the magnitude of the bias current $I_{bias}$ and the current through the magnetic field control line $I_{CL}$; consequently, the power and frequency of electromagnetic radiation can be controlled.

A theoretical description of the LJJ operation is conventionally provided using the phenomenological sine–Gordon equation [38, 57, 58]; this model yields a qualitative description of topological excitations (solitons) in Josephson junctions, but does not provide a quantitative relationship between tunnel currents and electromagnetic radiation in a distributed junction and does not take into account the energy gap of superconductors. To accurately describe the generation processes in the LJJ, a microscopic model [59, 60] has been developed based on the theory of microscopic quantum tunneling. Such a model allows one to quantitatively describe the features of real structures in the case of both symmetric Nb–$AlO_x$–Nb [59] junctions and asymmetric Nb–AlN–NbN structures [60]. The results calculated in these models, including the features of the current-voltage characteristics, are in good agreement with the experimental data [59, 60].

In early studies, radiation from LJJs was observed at frequencies of the order of 10 GHz [57, 61, 62] when operating at zero-field steps in Nb–$NbO_x$–Pb(InAu) junctions; the measured power was 1–10 pW, and the emission linewidth ranged from 0.1 to 50 MHz. Later, the emission frequency was increased to several tens of gigahertz, and integrated superconductor detectors were used for measurements. In [63], this technique was used to estimate the emission power of 100 pW at a frequency of 75 GHz. Then, a series of papers [37–40] were published on the development of a vortex flow generator in a junction with PbIn/Au electrodes in a magnetic field (Flux-flow type Josephson oscillator). Using an integrated superconductor detector, the power was estimated to be about 1 μW in the frequency range from 100 to 400 GHz.

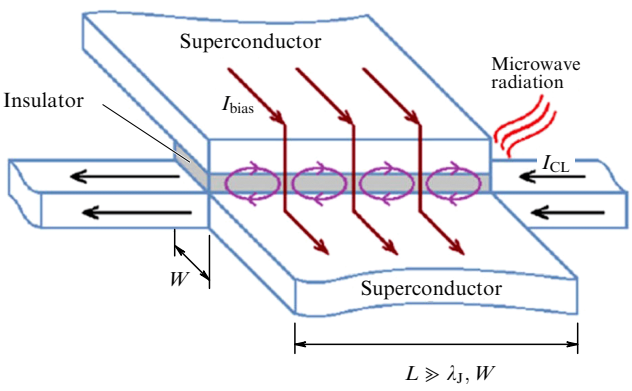


**Figure 1.** Schematic representation of LJJ-based oscillator.

Measurements conducted at Chalmers University [64, 65] at frequencies of about 300 GHz yielded a combined linewidth of the radiation of two LJJ generators, the signals of which were fed to an integrated SIS mixer. Its value was 2.1 MHz, and the incoming power of one LJJ generator, estimated by pumping the SIS mixer, was 430 nW at a frequency of 320 GHz. The integrated circuit was manufactured by standard microelectronics methods based on a three-layer $Nb-NbO_x-PbBi$ structure.

### 2.3 Generators based on high-temperature superconductors

An alternative option for creating THz-range generators is to use structures based on layered high-temperature superconductors. In the $Bi_2Sr_2CaCu_2O_{8+d}$ (BSCCO) compound, superconductivity with a critical temperature $T_c$ of about 90 K is provided by $CuO_2$ layers 0.3 nm thick, which are separated by barrier layers of SrO and BiO with a total thickness of 1.5 nm, forming a Josephson weak link. Thus, a single crystal 1 μm thick forms a stack of approximately 670 natural Josephson junctions with the highest possible packing density. The structure 'cut' from such a single crystal using nanometer-scale technologies is commonly called a mesa. Study [42] was the first to report the observation of microwave generation (about 10 GHz) from a layered structure of a single crystal based on a BSCCO mesa. However, it was only after the publication in *Science* in 2007 of an article [43] on the experimental observation of radiation at frequencies up to 600 GHz that a real boom in the development of generators based on BSCCO began. Several hundred articles were published annually devoted to both theoretical studies of the mechanisms occurring inside the complex multiparameter system of the generator and experimental studies of the radiating, thermal, and resonance properties of these structures.

The properties of THz radiation were shown to depend extremely strongly on the concentration of charge carriers, which changes due to doping or dedoping by current injection. THz radiation from natural arrays of Josephson junctions was experimentally studied in detail to reveal the relationship of the radiation frequency with various resonator modes. Of extreme importance for obtaining radiation at frequencies of the order of one THz and higher is good heat dissipation from the mesa structure [44–47]. Methods have been developed to obtain BSCCO arrays of Josephson junctions embedded between gold electrodes, so-called gold-BSCCO-gold (GBG) structures. An important role in generation from mesa structures is played by the 'hot spot'; a difference in conductivity between the cold and hot parts of the mesa leads to reflection of the electromagnetic wave from the boundary of the 'hot spot,' which can perform as an additional shunt that facilitates synchronization of the junctions in the array. The measured generation frequency is in the range of 0.2–2.4 THz; for the best mesa generators, the radiation power achieved was on the order of tens of μW [44–47]. It should be noted that the radiation was usually measured using semiconductor bolometers (based on Si or Ge) and a low spectral resolution of the order of one GHz.

We were the first to directly measure emission spectra of BSCCO mesa structures [44] using a superconducting integral spectrometer [21, 35, 36]. It was shown that the BSCCO generator exhibits the best spectral characteristics in the 'high bias' mode in the presence of a 'hot spot.' Typical values of the BSCCO generator linewidth, measured in the 'high bias' mode, were 10–100 MHz (Fig. 2a); the shape of the spectral line is Lorentzian with a high degree of accuracy. In the 'low bias' mode, the structure emits powerful broadband noise; the emission linewidth is about one GHz (Fig. 2b). In the range from 450 to 740 GHz, the spectral characteristics of the emission of HTS mesa structures were measured at temperatures from 4.2 to 55 K (Fig. 2c); the minimum emission linewidth of 7 MHz and power of 1–2 μW were obtained.

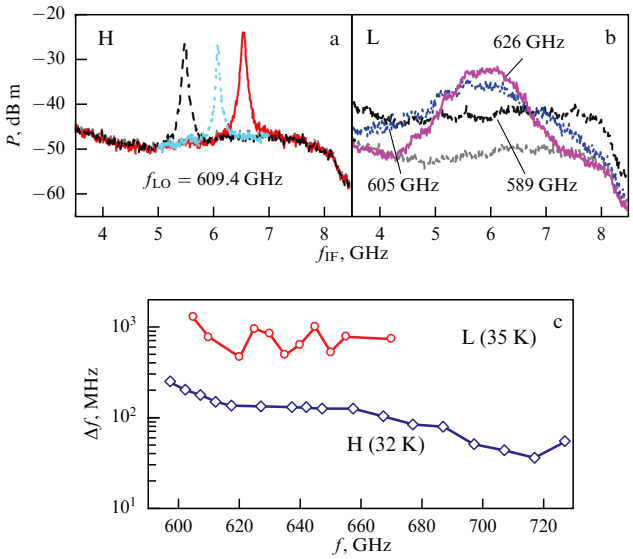


**Figure 2.** Emission spectra of oscillator based on BSCCO mesa structures in (a) high and (b) low bias current mode; (c) frequency dependence of radiation linewidth [44].

## 3. Integrated local oscillator based on distributed Josephson tunnel junctions

Usually employed as a heterodyne in THz and sub-THz receivers is an external source, the choice of which is currently fairly limited and has broadened only slightly over the past twenty years. Backward-wave oscillator (BWOs), which have relatively high power and span the range from 70 GHz to 1.5 THz, are bulky and require a high-voltage power supply and strong magnetic fields of about one Tesla to operate. Moreover, mass production of BWOs ceased more than three decades ago, and they are not commercially available due to the complexity of the technology. Currently, sources based on quantum cascade lasers are gaining popularity, but their operating range starts only from 1.5 THz, and the tuning band usually does not exceed 1% [66, 67]. Photomixers operating at the difference frequency of two lasers feature a wider band; their operating range extends to 2 THz, but the power is fairly low, and the conversion efficiency decreases exponentially with increasing frequency [68, 69]. Frequency multipliers based on Schottky diodes are widely and successfully used [30, 31], but, like photomixers, their efficiency significantly decreases at frequencies above one THz. The main problem is that THz-range multipliers and power amplifiers for frequencies of the order of 100 GHz required for pumping such multipliers are not commercially available in Russia. All of the above necessitates the development of alternative THz-range oscillators, one of the most developed of which is the LJJ-based superconducting THz-range oscillator [21, 35, 36].

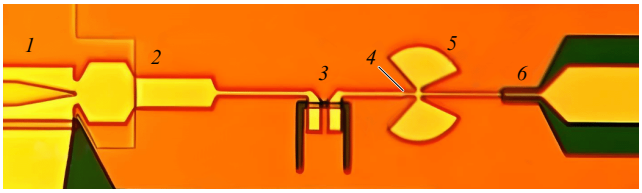


**Figure 3.** Image of integrated structure for studying emission from LJJ-based oscillator. Numbers indicate: *1* — oscillator (only a small part of Long Josephson junction with narrowing is shown); *2* — three-stage impedance transformer; *3* — DC block; *4* — SIS junction with inductive section for tuning SIS junction capacitance in operating frequency range; *5* — radial stubs; *6* — output coplanar line [72].

### 3.1 Development and main characteristics of superconducting local oscillator

To operate as part of an integrated receiver, the frequency should be tunable in a wide range and the power sufficient for efficient pumping of the SIS mixer [21, 35, 36]. In addition, for most practical applications, a high spectral resolution better than $10^{-6}$ is needed; this requires phase locking of the superconducting local oscillator (SLO) to a stable reference synthesizer. To study the superconducting local oscillator, integrated structures were developed that also contain an SIS detector of terahertz radiation [33, 37, 65, 70–72]. An image of a version of the integrated structure is presented in Fig. 3.

Studies were conducted on integrated circuits based on Nb–$AlO_x$–Nb and Nb–AlN–NbN tunnel structures. The technology for producing superconducting integrated structures based on high-quality tunnel junctions was developed and optimized at the Kotelnikov Institute of Radio Engineering and Electronics of the Russian Academy of Sciences [73–75]. This technology was tested in the production of low-noise THz-range receivers for radio astronomy and integrated receivers for atmospheric monitoring and laboratory applications [21, 75]. Equipment provided by the Cryointegral Unique Research Facility (the Technological and Measurement Complex for the Production of Superconducting Nanosystems Based on New Materials) was used to produce the structures [76]. This complex is unique and, in fact, the only one in the Russian Federation which can manufacture high-quality niobium-based tunnel junctions.

The effect of the terahertz generator radiation was detected by the change in the current-voltage characteristic of the superconducting detector; in this way, it is possible not only to detect the radiation, but also to estimate the signal power using the Tucker–Feldman model [16]. It should be noted that the SIS junction with a barrier thickness of about 1 nm has a high specific capacitance $C_{\text{spec}}$ (approximately 0.08 pF $\mu m^{-2}$); this leads to significant shunting of the nonlinear resistance of the junction $R_{\text{RF}}(V)$ at high frequency. The parasitic capacitance can be 'tuned out' at the operating frequency by connecting a small inductance, usually formed by a section of microstrip line several micrometers long. The inductance should not shunt the junction by direct current; to connect the inductance only at a high frequency, a 'blocking' capacitance is used, which can be realized using broadband radial short-circuiters (see Fig. 3).

A family of IVCs of a LJJ generator based on the Nb–Al/$AlO_x$–Nb structure measured in various magnetic fields is presented in Fig. 4. The color scale at each operating

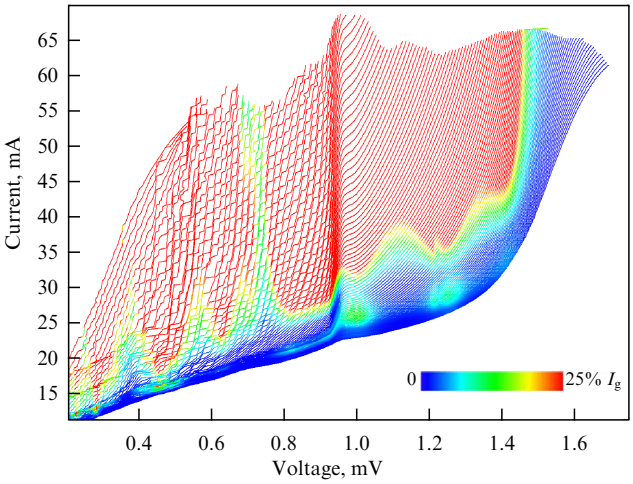


**Figure 4.** Families of LJJ IVCs based on Nb–Al/$AlO_x$–Nb structures, measured at various magnetic field values. Colormap shows level of increase in direct current (receiving microwave signal) from SIS mixer induced by radiation from LJJ generator (as a percentage of jump in mixer quasiparticle current $I_g$ at the gap voltage $V_g$).

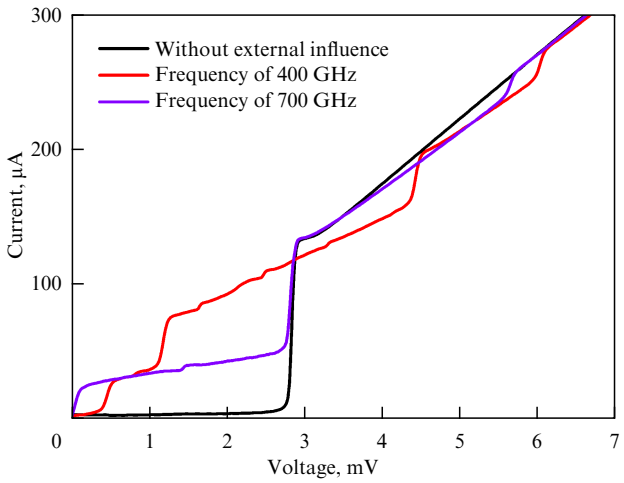


**Figure 5.** IVC of Nb–Al/$AlO_x$–Nb tunnel junction with an area of 1.4 $\mu m^2$; black curve in figure shows autonomous IVC, and colored curves present IVCs under the influence of a microwave signal from LJJ generator at frequencies of 400 and 700 GHz.

point on the IVC generator shows the measured values of the quasiparticle pump current of the integral SIS mixer (Fig. 5). Under the effect of microwave radiation incoming from the LJJ generator, quasiparticle steps arise on the IVC of the SIS mixer on both sides of the gap singularity at the voltage $V_g$, which are separated from $V_g$ by a multiple of $hf/e$, corresponding to the quantum energy of the incoming photons [16]. Tunneling of quasiparticles under the influence of external microwave radiation is called photon assisted tunneling. The current value is measured at a constant bias voltage of the SIS mixer slightly below $V_g$ and is normalized to the value of the current jump on the gap $I_g$. The red areas on the IVC of the generator correspond to the parameters at which the growth of the SIS mixer quasiparticle current exceeds 25% of its current jump at the gap voltage. This level is slightly higher than the optimum for the mixer operation. Figure 6 displays the dependence of the SIS mixer pump current on the frequency of LJJ, demonstrating

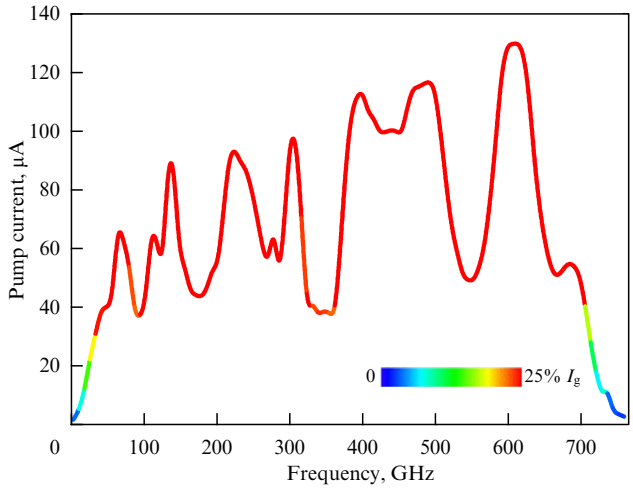


**Figure 6.** Measured maximum pump current of SIS mixer, measured at a voltage of 2.5 mV, as a function of LJJ frequency (colors show pump level as percentage of jump in mixer quasiparticle current $I_g$ at the gap voltage $V_g$).

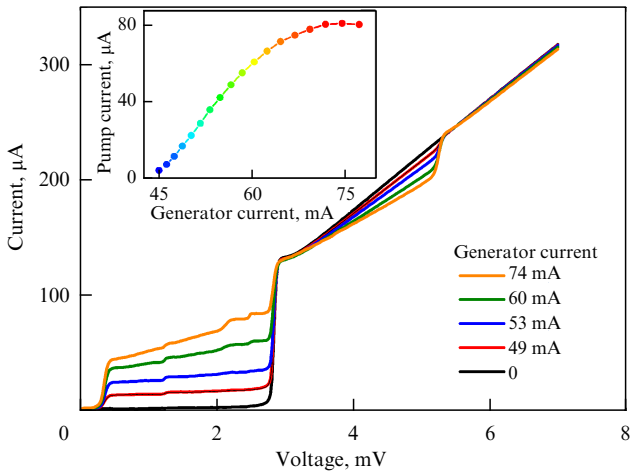


**Figure 7.** IVC family of SIS junction at various levels of microwave power incoming from LJJ generator current at a frequency of 600 GHz [72]. Inset: SIS mixer pump current as a function of LJJ bias current.

the wide frequency range of operation of both the LJJ-based generator and the matching circuits [77].

It is worth mentioning that the LJJ operation depends on the modes of junction operation, which impacts the motion of the Josephson vortices (fluxons) inside the junction. At voltages $V < V_g/3$ (where $V_g$ is the gap voltage), a resonant mode with a small parameter of the electromagnetic wave attenuation in the junction $\alpha$ arises, forming standing waves with modes

$$f_m = m\,\frac{\pi c_{SW}}{L}\,, \tag{2}$$

where $m$ is the mode number, $c_{SW}$ is the Swihart velocity, and $L$ is the junction length. This leads to the appearance of Fiske resonant steps on the VAC at voltages

$$V_m = m\,\frac{hc_{SW}}{4eL}\,, \tag{3}$$

where $h$ is the Planck constant, and $e$ is the electron charge; such steps hinder smooth tuning of the generator frequency due to the absence of operating points between the steps (see Fig. 4). At $V \approx V_g/3$, the Josephson self-coupling (JSC) effect appears, caused by the absorption of radiation by quasiparticles [78]. As a result, the amplitude of the quasiparticle current increases at voltages

$$V_{JSC} = \frac{V_g}{2n+1} \tag{4}$$

(the effect is most pronounced at $n = 1$, $V_{JSC} = V_g/3$), and the attenuation coefficient $\alpha$ increases. At $\alpha L/\lambda_J > 1$, the Fiske steps disappear, and the LJJ switches to the viscous vortex flow mode, in which the differential resistance changes monotonically, which allows smooth tuning of the generator frequency over a wide range. In Figure 4, the resonant structures (Fiske steps) and the region of transition to the JSC mode (dense structures in the region of approximately 0.95 mV) render the indicated effects.

The possibility of adjusting the power of the LJJ generator is illustrated in Fig. 7, which shows the IVC of the SIS mixer, measured by changing the current $I_{bias}$ flowing through the generator while maintaining a constant generation frequency by adjusting the current through the magnetic field control line $I_{CL}$. This adjustment was maintained by the automated IRTECON (Integrated Receiver TEst and CONtrol) system [79]. The inset to the figure shows the dependence of the pump current at a voltage of 2.5 mV on the current through the generator $I_{bias}$.

The use of the SIS junction as a mixer allows one to measure the radiation spectrum of the integrated heterodyne generator [65, 71], the SIS junction being used as a harmonic mixer (HM) with a high harmonic number [80]. The signal from the reference synthesizer $f_{SYNT}$ with a frequency of about 20 GHz is fed to the SIS junction, in which the $n$th harmonic of the synthesizer signal is mixed with the SLO signal with a frequency of $f_{SLO}$. The signal at intermediate frequency $f_{IF}$ about 1 GHz

$$f_{IF} = \pm\left(f_{SLO} - nf_{SYNT}\right) \tag{5}$$

is amplified by a cryogenic HEMT amplifier (noise temperature of approximately 5 K, gain of 30 dB), is output from the cryostat and, after an additional amplifier, the signal is branched to a spectrum analyzer for recording spectra and to a phase-lock-loop frequency control (PLL) system with an additional frequency detector. A frequency detector with a control band of about 10 kHz stabilizes the frequency, removing low-frequency interference and temperature drifts (Fig. 8). The autonomous radiation line is shown in blue in the figure; the line width is 1 MHz, and the signal-to-noise ratio is 45 dB. When using the PLL system, the incoming signal is compared with the reference signal of 400 MHz from the synthesizer, while the phase error signal is fed to the LJJ to stabilize its frequency. The result is shown in Fig. 8 (red curve); the ratio of the signal in the central peak to the total power is 97.5%.

The relative phase noise of the SLO in the PLL mode depending on the detuning from the central frequency is shown in Fig. 9 [72]. This noise is measured relative to the reference synthesizer. To calculate the absolute (total) phase noise, it is necessary to add the noise of the reference synthesizer multiplied by the square of the harmonic number (in this case, $n = 20$). The absolute phase noise value is shown in the figure by the red curve.

Most practical applications require continuous frequency tuning of the superconducting generator at an

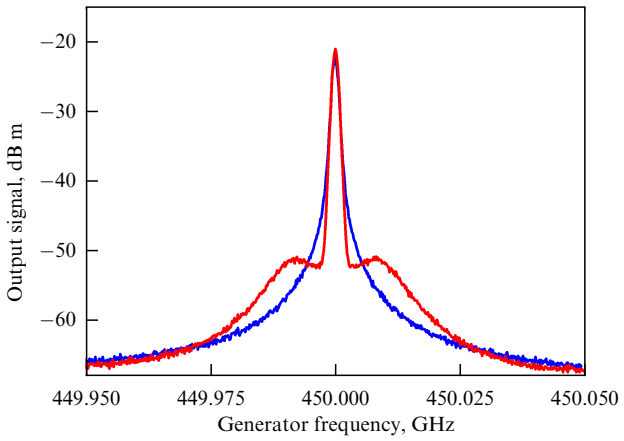


**Figure 8.** SLO radiation spectrum at frequency of 450 GHz measured using harmonic mixer in frequency stabilization mode (blue curve) and in phase lock mode (red curve) with a spectrum analyzer resolution (resolution band-width) RBW = 1 MHz [72].

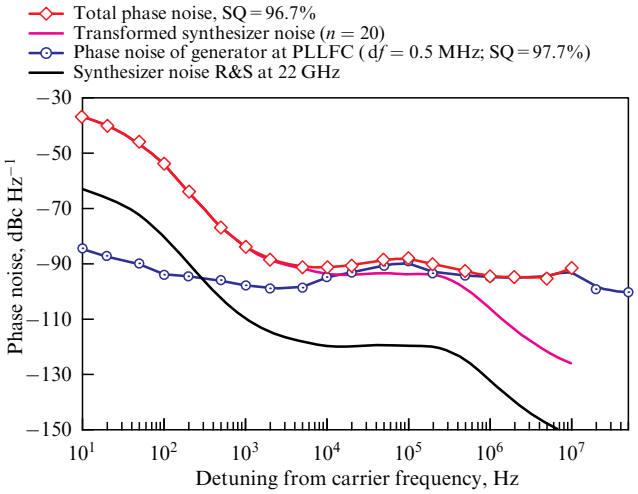


**Figure 9.** Phase noise of LJJ generator at a frequency of 450 GHz as a function of detuning from carrier frequency (blue circles). Black solid curve shows phase noise of reference synthesizer at fundamental frequency of 22.48 GHz; magenta solid curve, at 20th harmonic, and red diamonds represent total (absolute) phase noise of LJJ oscillator in PLL mode taking into account the contribution of synthesizer noise [72].

arbitrary bias current. This requirement is naturally fulfilled in the flux flow mode, while, when operating in the resonant mode, stable generation is only possible at the Fiske steps, the distance between which in frequency is tens of GHz. To solve this problem, it was proposed to introduce additional absorbing layers of molybdenum into the LJJ design to increase the attenuation parameter $\alpha$ [81]. This solution facilitates dissipation of the reflected electromagnetic wave inside the junction and smoothing of the resonant step structure at the IVC.

Figure 10 presents a direct comparison of the dependences of the differential resistance $R_d$ on the voltage at the LJJ for conventional (blue) and modernized (red) generator designs. The inset shows a structural diagram of the modernized LJJ generator with absorbing layers at the nonradiating end of the generator, marked in green. It is clearly seen that the plot of the $R_d(V)$ dependence for a LJJ with absorbing resistors has become smoother, without rapid shifts. The value in the voltage range of 0.6–0.9 mV varies by no more than 10 mΩ,

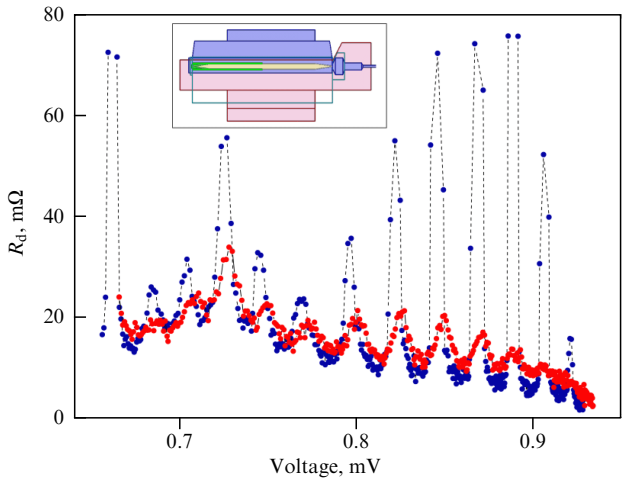


**Figure 10.** Dependences of differential resistance for conventional LJJ oscillator (shown in blue) and oscillator with absorbing resistive layers (red).

which approximately corresponds to a 10-MHz change in the width of the generator emission spectrum line. The generation line width was in the range of 4–12 MHz, which made it possible to implement the PLL mode in the entire frequency range at the optimal LJJ power for pumping the SIS [81].

A LJJ-based generator was successfully used as a heterodyne source in a unique device — a superconducting integrated receiver (SIR), which still has no counterpart in the world in terms of the compactness of the implementation of key elements and the parameters achieved [21, 81–86]. The SIR concept, which was first proposed at the Kotelnikov Institute of Radio Engineering and Electronics of the Russian Academy of Sciences, is that the main elements of the superheterodyne receiver — a LJJ-based reference generator and a receiving element based on an SIS junction — are integrated on a single 4×4-mm microcircuit. The receiving SIS detector, in turn, is integrated into a double dipole or slot antenna, and an additional harmonic SIS mixer in the harmonic mixing section is designed on the SIR chip for frequency and phase stabilization of the LJJ. The complex SIR instrument, including optical and mechanical parts, which operates in the 480–700 GHz range, was developed together with researchers from the Netherlands Institute for Space Research as part of the TErahertz Limb Sounder (TELIS) project to study the gas components of Earth's atmosphere and was several times successfully launched aboard a high-altitude balloon [35, 84–86]. The tuning of the LJJ operating frequency in a broad range and high integration of elements on a single microcircuit enabled studying a huge number of compounds in the atmosphere with spectral absorption and emission lines in the THz region — ClO, BrO, $O_3$, HCl, HOCl, $H_2O$ and its isotopes, $HO_2$, NO, $N_2O$, $HNO_3$, $CH_3Cl$, HCN, and many others — using a single receiver.

### 3.2 Generator of THz radiation into open space

After the LJJ-based generator was developed and thoroughly studied, experimentally tested with the PLL system as part of an integrated sub-THz receiver, and successfully tested during scientific launches on a high-altitude balloon, the idea of developing a source based on a LJJ radiating into open space arose quite naturally.

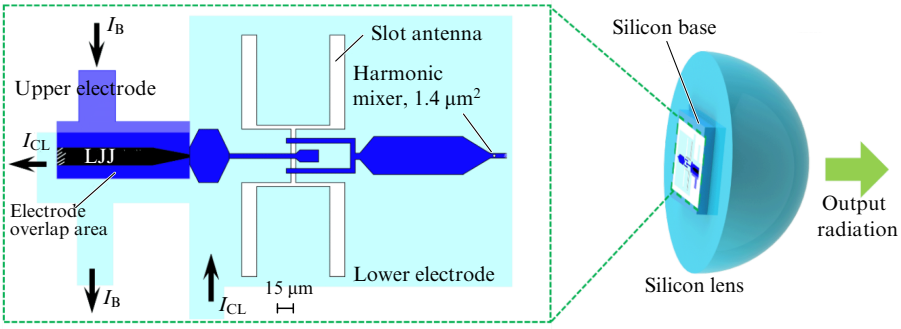


**Figure 11.** Schematic design of the LJJ-based open-space radiation source for center frequency of 450 GHz: on left is central part of integrated circuit; on right is diagram of mounting on silicon lens.

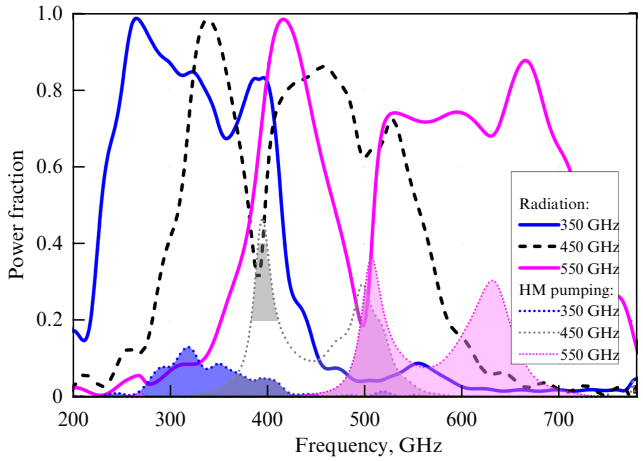


**Figure 12.** Results of numerical simulation of three integrated source designs: displayed are fraction of power emitted into open space (curves without shading in lower region) and fraction of HM pumping power (curves with lower region shaded) from total output power of LJJ.

Several LJJ-based oscillator designs have been developed, radiating into open space in various frequency ranges: 250–450 GHz, 320–550 GHz, and 400–700 GHz, spanning a total frequency band from 250 to 700 GHz. The key idea of the concept is, first, to output the oscillator radiation from the transition region into open space using a transmitting slot antenna, and second, to provide a feedback mechanism for frequency and phase stabilization using a harmonic mixer and a PLL system. Figure 11 presents the general concept of the cryogenic part of the source, while Fig. 12 displays the frequency characteristics of three designs with a center frequency of 350 GHz, 450 GHz, and 550 GHz [87–91]. It should be noted that the source tuning bandwidth of about 30–50% is set in this concept by the operating bandwidth of the antenna, which is significantly narrower than the tuning bandwidth of the LJJ sample, which is up to 100% (from 200 to 700 GHz).

For successful operation of the PLL system, it is sufficient to pump the harmonic mixer with a relatively small power (no more than 10–15% of the $I_g$ of the mixer IVC) [72]; therefore, the integrated circuit of the generator is designed in such a way that more than 70% of the LJJ output power goes to the transmitting antenna and is radiated into open space, while no more than 20–30% of the power is branched off to the harmonic mixer in the feedback circuit (Fig. 12). LJJs can be made on the basis of Nb–$AlO_x$–Nb or Nb–AlN–NbN structures; the choice of materials for the electrodes of the three-layer structure affects the frequency ranges of the resonant mode (Fiske-steps mode) and the viscous vortex flow mode and, consequently, the characteristic width of the generation line in various frequency ranges. The cryogenic module with the generator is mounted in a cryostat with an operating temperature of 4.2 K.

The output characteristics of the generator were studied using a wide range of various methods. The spectral line of that small part of the LJJ signal that entered the harmonic mixer was measured at an intermediate frequency in the 0–800-MHz band similarly to the method described in Section 3.1; the linewidth ranged from hundreds of kHz to several MHz without a phase-locked loop (in the autonomous mode). One of the key characteristics of the developed source is the spectral line of the signal emitted into open space. This signal was recorded by a superconducting integrated receiver in its operating band of 480–700 GHz, the local oscillator of which is made of the same LJJ as the source under study. The recorded spectral characteristics of the signal in open space differ from the radiation characteristics in the feedback loop only by the correction of the spectral characteristic of the receiver's local oscillator (signal convolution) [87, 88]. This implies that the terahertz path from the generator to open space, consisting of a microstrip line, a slot antenna, and a lens, does not introduce additional noise or distortions into the emitted spectrum.

The tuning range of the source was studied using a broadband semiconductor cryogenic bolometer based on silicon with an operating temperature of 4.2 K and a sensitivity to noise equivalent power (NEP) at the level of $1.3 \times 10^{-13}$ W $Hz^{-1/2}$ [89, 90]. Study of the tuning range for three experimental generator designs for operation in three frequency ranges yielded results that turned out to be quite close to the numerical calculations (see Fig. 12). Thus, it was shown that the developed calculation model allows designing a source circuit based on a LJJ with wide tuning for any target frequency up to 700 GHz by only adjusting the antenna topology and matching path without changing the design of the LJJ itself or the quasi-optical path.

The absolute value of the signal power emitted into the open space was measured based on the experimentally known IVC of the harmonic mixer in the feedback loop under the influence of radiation. The Thien–Gordon model, the methods reported in [16, 92], and the measured IVC of the SIS junction under the influence of pumping by an external signal were used to obtain the LJJ power value at this frequency. Next, based on the determined value of the harmonic mixer pumping power and the previously obtained ratio of the pumping and

radiation powers, the power radiated into the open space is estimated. The method described yielded power values from about 0.5 μW at frequencies of 600–700 GHz to 2–3 μW at frequencies of 320–380 GHz [91].

The developed source, in addition to its properties unique in terms of tuning range and integrability into a cryogenic system, made it possible to conduct direct experimental observations of Josephson generation harmonics [93, 94]. The existence of higher harmonics ($N = 2$ and higher) was predicted and numerically described [95, 96] several decades ago during the peak of theoretical studies on the Josephson effect. Only indirect experimental confirmation of the presence of generation harmonics that followed from observations of features on the IVC [97] or from the results of multiplying the frequency of an external signal in the harmonic mixer mode [98] was available. However, since power radiated at higher harmonics is extremely low and sub-THz receivers were virtually unavailable until the 1990s, no direct experimental observations were made. In studies [93, 94], we used an open-space radiation generator developed by our research team and a broadband THz Fourier spectrometer based on a two-beam Michelson interferometer with a cryogenic bolometric detector to demonstrate quite clearly the presence of the second and, in some cases, the third harmonics of radiation into open space. In [91, 99], the feasibility of application of the LJJ as an active source for terahertz spectroscopy of gases was clearly demonstrated.

## 4. Generator based on array of Josephson junctions in a coplanar line

Interest in studying arrays of Josephson junctions is due to the fact that arrays can feature some advantages over LJJs. In particular, in a LJJ, the exact shape of the IVC alters from one thermal cycling to another [35, 36], so the preliminary tuning of the local oscillator even when using an automated system requires some time (about 1 min). For Josephson junction arrays, such a limitation is not expected. At the same time, manufacturing large Josephson junction arrays is much more complex, since a small spread of junction parameters within a single chip is needed for synchronous operation of all junctions. Below are the results of studies of Josephson junction arrays carried out by the authors recently.

### 4.1 Design and main characteristics of the generator

The image of one of the studied samples with a generator based on an array of 350 Josephson junctions is presented in Fig. 13a. The array is a coplanar line with junctions built into the central electrode. The proposed topology, to the best of our knowledge, is considered for the first time. In our opinion, it is the choice of this particular array topology that allowed us to achieve synchronization between the junctions and efficient generation in a wide frequency band. In addition, the use of a coplanar line allows us to reduce losses in the electrodes (compared to the microstrip design and a LJJ) when operating at frequencies close to the band gap frequency, especially for junctions with a high current density. A detailed theoretical description of the synchronization in the array and the related generation features is a subject of further research.

The radiation power of the array is determined by the pump current of the detector in the form of a single SIS junction of small area (1–1.5 μm$^2$). To ensure an independent DC connection of the detector and generator, a gap in

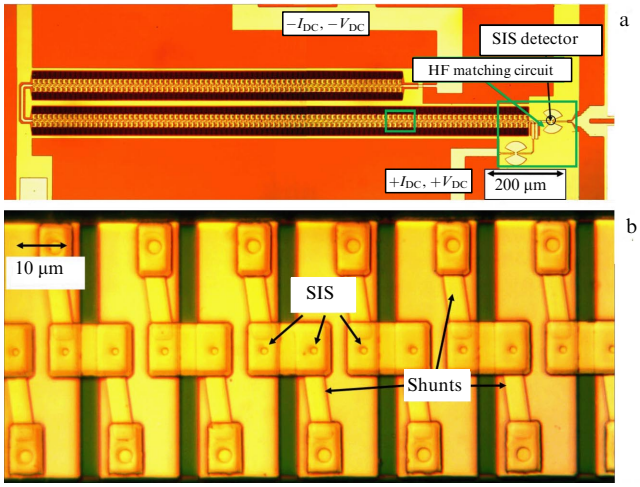


**Figure 13.** (a) Image of chip with array of 350 Josephson junctions. (b) Enlarged image of junctions in the array.

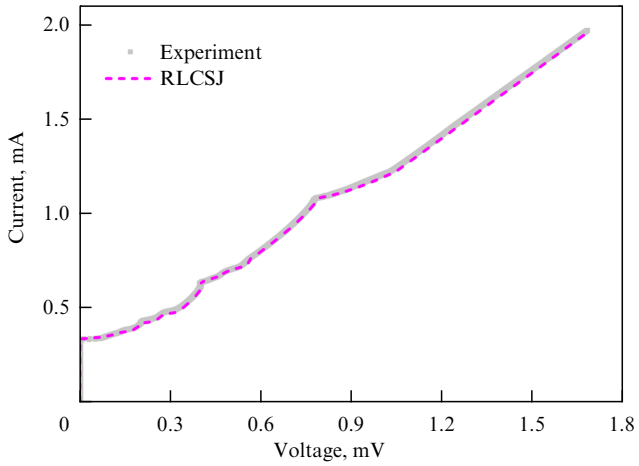


**Figure 14.** IVC of a single junction shunted by thin-film resistor. Experimental IVC (gray dots) and theoretical dependence obtained using RLCSJ model (dashed line).

the form of a slot antenna is provided between them. An impedance transformer is installed to match the impedances of the detector and the gap between them. The impedances of the array and the antenna are approximately the same, so there is no need for an additional matching circuit. The DC power supply line of the array is designed to limit the radiation drift in the operating range (from 300 to 700 GHz).

Each junction is shunted with a thin-film molybdenum resistor, which is in the normal state at the experimental temperature (4–5 K) (Fig. 13b). The shunt resistance was selected in such a way as to obtain the McCumber parameter $\beta_C$ of an individual junction of less than 0.5 and to ensure a hysteresis-free behavior of the IVC. The IVC of one shunted Nb–Al/AlN–NbN junction is shown in Fig. 14 in solid gray. The IVC has a number of features associated with the excitation of $LC$-resonances, where $C$ is the junction capacitance, and $L$ is the inductance, which is the sum of the geometric inductance of the shunt and the nonlinear inductance of the junction. For a theoretical description of the IVC, the RLCSJ model [32] was used, which takes into account not only the capacitance of the SIS junction and the shunt resistance, but also its geometric inductance (see the dashed curve in Fig. 14). The theoretical and experimental

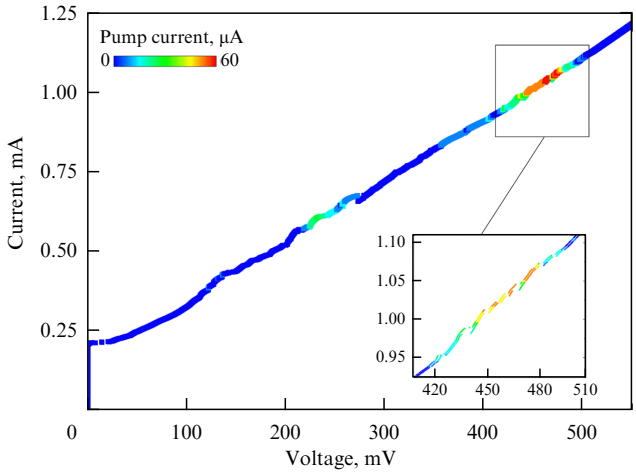


**Figure 15.** IVC of array of 350 shunted Nb–Al/AlN–NbN Josephson junctions with area of 2.8 μm$^2$. Tunneling current density is ∼ 13 kA cm$^{-2}$. Colors show pump current of SIS detector.

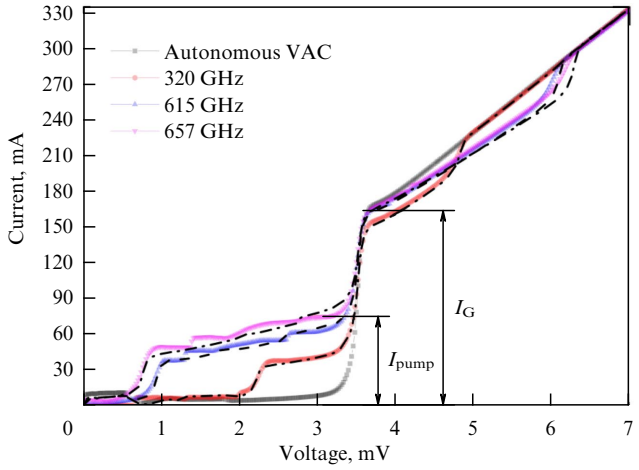


**Figure 16.** Family of SIS detector IVCs under the action of radiation from array. Gray dots show VAC without pumping, and colored lines represent pumped VAC and at corresponding frequencies. Black dashed-dotted curves show calculated VAC and those obtained using formulas of Tucker–Feldman model [16].

curves almost coincide for the parameters $R_{sh} = 0.87$ Ω, $L_{sh} = 1.75$ pH, $C = 338$ fF, and $I_c = 0.333$ mA, where $R_{sh}$ and $L_{sh}$ are the resistance and geometric inductance of the shunt, and $I_c$ is the critical current through the junction.

The IVC of an array of 350 Nb–Al/AlN–NbN junctions is displayed in Fig. 15. The features characteristic of the IVC of a single shunted junction are blurred, apparently due to a small spread in the parameters of individual junctions that form the array. Additional features that arise on the IVC of the array are due to geometric resonances along the entire length of the structure. The characteristic distance between the steps is ∼ 17 GHz, which is in qualitative agreement with the frequency interval between resonances in a coplanar line 3.5 mm long. The IVC also includes sections with a small hysteresis; their position alters with a change in the junction parameters; for example, with an increase in temperature, the sections with hysteresis shift to lower voltages. It is possible that this effect can be used in the future as an additional tool for controlling the array dynamics and adjusting the operating region. The colors in Fig. 15 indicate the value of the SIS detector pump current at a voltage of 3 mV.

Figure 16 presents the IVC of an SIS detector; when a signal from the array is applied, quasiparticle current steps arise on the detector IVC at characteristic voltages $V_{gap} - hf/e$, where $V_{gap}$ is the gap voltage and $f$ is the frequency of the detected signal. The critical current is partially suppressed by the external magnetic field. The features near 1.3 mV, 2.6 mV, and 3.9 mV are the Shapiro steps that emerge on the IVC due to incomplete suppression of $I_c$. The pumped IVCs calculated using the Tucker–Feldman model formulas [16] are shown as black dashed curves superimposed on experimental data. Minor disagreements between the model and experimental IVCs are caused by the impedance mismatch of the SIS detector and the circuit external to it [100]. The LJJ generation frequency at the operating points was verified using the position of the Shapiro steps.

Figure 17 displays the frequency dependence of the pump current for samples with $N = 350$ junctions with tunneling current densities of 5, 13, and 20 kA cm$^{-2}$. A total of 4 series of experimental samples were made. The

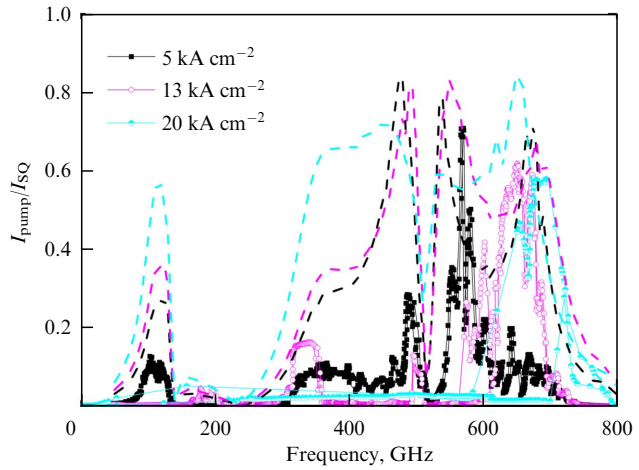


**Figure 17.** Frequency dependence of pump current in samples with various tunneling current densities. Experimental data are shown by corresponding markers; dashed curves show coefficients $S_{21}$ for matching circuit between array and SIS detector calculated in ANSYS HFSS.

samples in each series differ from each other in the number of junctions in the array and their area. The shunt resistance in each series was selected so that the McCumber parameter $\beta_c$ was less than 0.5 to ensure hysteresis-free behavior of the IVC array.

In the series with a tunneling current density of junctions of 5 kA cm$^{-2}$, the width of the operating band is determined by the transfer characteristic of the matching circuit (see the corresponding curves in Fig. 17). The matching circuit was calculated using the ANSYS HFSS 3D numerical modeling program. The method for modeling superconducting structures in the ANSYS HFSS program is described in detail in [101]. The dip at frequencies near 500 GHz, observed both in calculations and in the experiment, is due to the power leak into the DC connection line of the array. In samples with a higher tunnel current density, the generation band turned out to be significantly narrower. For a series with a tunnel current density of 20 kA cm$^{-2}$, $\beta_c$ turned out to be 2.3, due to which a strong hysteresis was observed on the IVC, and synchronization was only achieved in a narrow range.

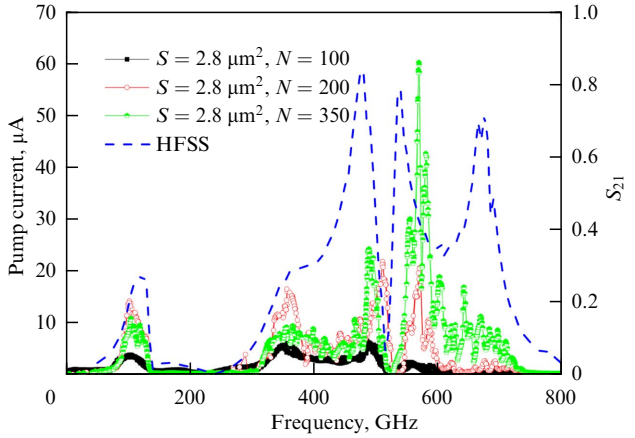


**Figure 18.** Frequency dependence of pump current in samples with 100, 200, and 350 Nb–Al/$AlO_x$–Nb junctions with area of 2.8 μm$^2$ and tunneling current density of 5 kA cm$^{-2}$. Dashed line shows frequency dependence of coefficient $S_{21}$ of matching circuit between array and SIS detector calculated in ANSYS HFSS.

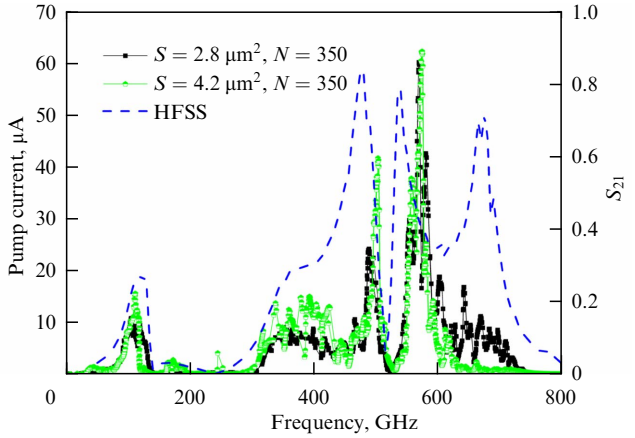


**Figure 19.** Frequency dependence of pump current in sample with 350 Nb–Al/$AlO_x$–Nb junctions with tunneling current density of 5 kA cm$^{-2}$ and areas of 2.8 and 4.2 μm$^2$. Dashed line shows frequency dependence of coefficient $S_{21}$ of matching circuit between array and SIS detector calculated in ANSYS HFSS.

Figure 18 displays the frequency dependence of the pump current for samples with $N = 100$, 200, and 350 Nb–Al/$AlO_x$–Nb junctions, a tunneling current density of $\sim 5$ kA cm$^{-2}$, and an area of 2.8 μm$^2$. With an increase in the number of junctions in the array, the maximum generation power increases faster than $N$. The irregularity of the dependences is most likely due to the occurrence of standing waves in the line and frequency locking at the corresponding operating points. In the sample with 350 junctions, the irregularity is most pronounced due to the higher generated power and, consequently, higher frequency locking efficiency. To eliminate this effect, samples with a matched load at the nonemitting end of the array are being designed.

Figure 19 presents the frequency dependences of the detector pump current for samples with arrays of 350 junctions with areas of 2.8 and 4.2 μm$^2$. The maximum operating frequency of the junction array with the larger area turned out to be somewhat lower, most likely due to the larger parasitic capacitance of the junctions. The average generation power higher in the junction array with the larger area, but the peak power turned out to be almost the same for the compared samples.

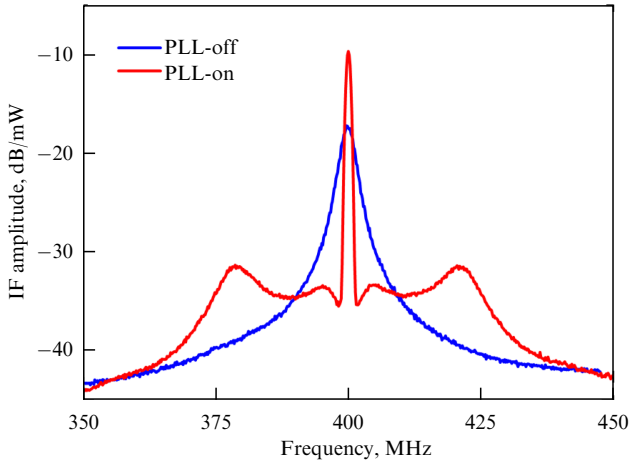


**Figure 20.** Signal spectrum at 650 GHz; blue curve represents autonomous generation line. Generation linewidth is about 3 MHz. Signal-to-noise ratio is 26 dB. Red curve represents spectrum with PLL system enabled. Spectral ratio is $\sim 87\%$.

### 4.2 Measurement of emission spectra and frequency stabilization modes

The proposed topology of lumped Josephson junction arrays made it possible to create a controlled tunable terahertz oscillator with a power sufficient for on-chip applications as a heterodyne generator in a superconducting integrated receiver. As already noted, for spectroscopic applications of SIRs, the frequency resolution of the receiver should be better than $10^{-6}$. To this end, the frequency and phase of the local oscillator radiation must be stabilized using an external PLL system.

The scheme used for frequency stabilization of the array is the same as for the PLL of a LJJ. The sample under study is placed in a vacuum volume of a cryostat filled with liquid helium. The SIS detector mixes the radiation from the array with harmonics of the signal from the synthesizer tuned to a frequency of about 18 GHz. In this case, the SIS detector operates as a harmonic mixer. The signal at the intermediate frequency is output from the cryostat to the input of the spectrum analyzer and the PLL input. Due to the feedback, the voltage on the array is adjusted depending on the difference between the IF signal and the PLL reference signal. In this way, both frequency and phase lock can be implemented. A more detailed description of the PLL system operation can be found, for example, in [102]. Preliminary measurements were carried out on an array of 350 junctions with an area of 2.8 μm$^2$ and a tunneling current density of 13 kA cm$^{-2}$. The radiation spectrum at a frequency of 650 GHz is shown in Fig. 20. The natural linewidth at this point was 3 MHz with a signal-to-noise ratio of 26 dB.

The feasibility of implementing a phase-locked loop of the superconducting oscillator based on the array of Josephson junctions from an external source has been experimentally demonstrated. To the best of our knowledge, this effect for arrays has been described for the first time. The spectral ratio of the oscillator in the PLL mode reached 87% already in the first experiments.

## 5. Conclusions

The superconducting oscillators explored in this study feature a wide operating band with the generation frequency tunable

by adjusting the voltage. LJJ-based oscillators have been studied for several years, and their design and parameters have been optimized; a superconducting integrated receiver was developed and tested, in which a LJJ was used as a local oscillator. It was shown that, if layers of normal metal are introduced in the LJJ-based oscillator, Fiske steps can be suppressed without significant deterioration of the spectral quality of the signal. In addition, it was shown that the LJJ can generate radiation into open space.

A new topology of a generator based on an array of Josephson junctions connected in series has been proposed, in which the array is built into the central electrode of a coplanar line. This topology enables the synchronization between the junctions and efficient generation at frequencies ranging from 100 to 700 GHz with a limitation due to the transmission characteristic of the matching circuit. Already in the first experiments, a generation linewidth at the best points of about 1 MHz was measured. The feasibility of implementing the PLL mode for a generator based on an array of Josephson junctions has been demonstrated for the first time. In further studies, the generation spectra of the arrays will be measured in more detail, and the generation linewidth will be compared with theoretical models. It is also planned to create arrays with a larger number of junctions and matching circuits with flatter characteristics.

The study was supported by the Ministry of Science and Higher Education of the Russian Federation (agreement no. 075-15-2024-538). The THz-range generators and the technology for their manufacture were developed with the support of the Russian Science Foundation (grant no. 23-79-00019, https://rscf.ru/project/23-79-00019/).

## References


1. Tinkham M *Introduction to Superconductivity* (New York: McGraw-Hill Book Co., 1975); Translated into Russian: *Vvedenie v Sverkhprovodimost'* (Moscow: Atomizdat, 1980)
2. Barone A, Paternó G *Physics and Applications of the Josephson Effect* (New York: John Wiley and Sons, 1982); Translated into Russian: *Effekt Dzhozefsona. Fizika i Primeneniya* (Moscow: Mir, 1984)
3. Likharev K K *Dynamics of Josephson Junctions and Circuits* (New York: Gordon and Breach Sci. Publ., 1986)
4. Clarke J, Braginski A I (Eds) *The SQUID Handbook*: *Applications of SQUIDs and SQUID Systems* (Hoboken, NJ: Wiley-VCH, 2006) https://doi.org/10.1002/9783527609956
5. Weinstock H (Ed.) *SQUID Sensors*: *Fundamentals, Fabrication and Applications* (NATO Science Ser. E, Vol. 329) (Dordrecht: Springer, 2012) https://doi.org/10.1007/978-94-011-5674-5
6. Semenov A D, Gol'tsman G N, Korneev A A *Physica C* **351** 349 (2001)
7. Gol'tsman G N et al. *Appl. Phys. Lett.* **79** 705 (2001)
8. Pernice W H P et al. *Nat. Commun.* **3** 1325 (2012)
9. Macklin C et al. *Science* **350** 307 (2015)
10. White T C et al. *Appl. Phys. Lett.* **106** 242601 (2015)
11. Aumentado J *IEEE Microwave Mag.* **21** (8) 45 (2020)
12. Likharev K K, Semenov V K *IEEE Trans. Appl. Supercond.* **1** (1) 3 (1991)
13. Bairamkulov R, De Micheli G *IEEE Circuits Syst. Mag.* **24** (2) 16 (2024)
14. Rey-de-Castro R C et al. *IEEE Trans. Appl. Supercond.* **11** 1014 (2001)
15. Klenov N V et al. *Low Temp. Phys.* **43** 789 (2017); *Fiz. Nizk. Temp.* **43** 991 (2017)
16. Tucker J R, Feldman M J *Rev. Mod. Phys.* **57** 1055 (1985)
17. Zmuidzinas J, Richards P L *Proc. IEEE* **92** 1597 (2004)
18. Tucker J *IEEE J. Quantum Electron.* **15** 1234 (1979)
19. Richards P L et al. *Appl. Phys. Lett.* **34** 345 (1979)
20. Kerr A R, Feldman M J, Pan S-K, in *Proc. of the Eighth Intern. Symp. on Space Terahertz Technology, Cambridge, MA, 25–27 March, 1997* (Eds R Blundell, E Tong) (Cambridge: Harvard Univ., 1997) p. 101
21. Filippenko L V et al. *Phys. Usp.* **67** 1139 (2024); *Usp. Fiz. Nauk* **194** 1207 (2024)
22. ALMA Observatory, https://www.almaobservatory.org/en/about-alma/
23. The Event Horizon Telescope, https://eventhorizontelescope.org/
24. Press Release (April 10, 2019): Astronomers Capture First Image of a Black Hole. The Event Horizon Telescope, https://eventhorizon-telescope.org/press-release-april-10-2019-astronomers-capture-first-image-black-hole
25. Akiyama K et al. (The Event Horizon Telescope Collab.) *Astron. Astrophys.* **681** A79 (2024)
26. Millimetron Space Observatory, http://millimetron.ru/index.php/en/
27. Novikov I D et al. *Phys. Usp.* **64** 386 (2021); *Usp. Fiz. Nauk* **191** 404 (2021)
28. Herschel Space Observatory, https://www.herschel.caltech.edu/
29. de Graauw Th et al. *Astron. Astrophys.* **518** L6 (2010)
30. Siles J V et al. *IEEE Trans. Terahertz Sci. Technol.* **8** 596 (2018)
31. Siles J V et al. *IEEE Trans. Terahertz Sci. Technol.* **14** 607 (2024)
32. NASA Jet Propulsion Laboratory. California Institute of Technology, https://www.jpl.nasa.gov/
33. Jain A K et al. *Phys. Rep.* **109** 309 (1984)
34. Darula M, Doderer T, Beuven S *Supercond. Sci. Technol.* **12** R1 (1999)
35. Koshelets V P et al., in *Fundamentals of Superconducting Nanoelectronics* (NanoScience and Technology, Ed. A Sidorenko) (Berlin: Springer, 2011) p. 263, https://doi.org/10.1007/978-3-642-20158-5_10
36. Dmitriev P N, Filippenko L V, Koshelets V P, in *Josephson Junctions. History, Devices, and Applications* (Eds E L Wolf et al.) (New York: Jenny Stanford Publ., 2017) p. 185
37. Nagatsuma T et al. *J. Appl. Phys.* **54** 3302 (1983)
38. Nagatsuma T et al. *J. Appl. Phys.* **56** 3284 (1984)
39. Nagatsuma T et al. *J. Appl. Phys.* **58** 441 (1985)
40. Qin J, Enpuku K, Yoshida K *J. Appl. Phys.* **63** 1130 (1988)
41. Koshelets V P et al. *IEEE Trans. Appl. Supercond.* **15** 960 (2005)
42. Kleiner R et al. *Phys. Rev. Lett.* **68** 2394 (1992)
43. Ozyuzer L et al. *Science* **318** 5854 1291 (2007)
44. Li M et al. *Phys. Rev. B* **86** 060505 (2012)
45. Welp U, Kadowaki K, Kleiner R *Nature Photon.* **7** 702 (2013)
46. Kakeya I, Wang H *Supercond. Sci. Technol.* **29** 073001 (2016)
47. Kleiner R, Wang H *J. Appl. Phys.* **126** 171101 (2019)
48. Wengler M J, Guan B, Track E K *IEEE Trans. Microwave Theory Tech.* **43** 984 (1995)
49. Song F et al. *Appl. Phys. Lett.* **95** 172501 (2009)
50. Han S et al. *Appl. Phys. Lett.* **64** 1424 (1994)
51. Booi P A A, Benz S P *Appl. Phys. Lett.* **68** 3799 (1996)
52. Cawthorne A B et al. *Phys. Rev. B* **60** 7575 (1999)
53. Galin M A et al. *Supercond. Sci. Technol.* **34** 075005 (2021)
54. Kawakami A, Uzawa Y, Wang Z *IEEE Trans. Appl. Supercond.* **9** 4554 (1999)
55. Golubov A A, Malomed B A, Ustinov A V *Phys. Rev. B* **54** 3047 (1996)
56. Ustinov A V, Kohlstedt H, Henne P *Phys. Rev. Lett.* **77** 3617 (1996)
57. Joergensen E et al. *Phys. Rev. Lett.* **49** 1093 (1982)
58. Zhang Y M, Wu P H *J. Appl. Phys.* **68** 4703 (1990)
59. Gulevich D R, Koshelets V P, Kusmartsev F V *Phys. Rev. B* **96** 024515 (2017)
60. Gulevich D R, Filippenko L V, Koshelets V P *J. Low Temp. Phys.* **194** 312 (2019)
61. Yanson I K, Svistunov V M, Dmitrienko I M *Sov. Phys. JETP* **21** 650 (1965); *Zh. Eksp. Teor. Fiz.* **48** 976 (1965)
62. Cirillo M, Lloyd F L *J. Appl. Phys.* **61** 2581 (1987)
63. Cirillo M et al. *J. Appl. Phys.* **65** 2376 (1989)
64. Zhang Y M, Winkler D, Claeson T *IEEE Trans. Appl. Supercond.* **3** 2520 (1993)
65. Zhang Y M, Winkler D, Claeson T *Appl. Phys. Lett.* **62** 3195 (1993)
66. Vijayraghavan K et al. *Nat. Commun.* **4** 2021 (2013)
67. Hayton D J et al. *Appl. Phys. Lett.* **103** 051115 (2013)
68. Nagatsuma T, Ito H, Ishibashi T *Laser Photon. Rev.* **3** 123 (2009)

69. Lu Q Y et al. *Appl. Phys. Lett.* **105** 201102 (2014) https://doi.org/10.1063/1.4902245
70. Koshelets V P et al. *IEEE Trans. Appl. Supercond.* **3** 2524 (1993)
71. Koshelets V P et al. *Appl. Phys. Lett.* **69** 699 (1996)
72. Dmitriev P N et al. *J. Commun. Technol. Electron.* **66** 473 (2021); *Radiotekh. Elektron.* **66** 410 (2021)
73. Filippenko L V et al. *IEEE Trans. Appl. Supercond.* **11** 816 (2001)
74. Dmitriev P N et al. *IEEE Trans. Appl. Supercond.* **13** 107 (2003)
75. Rudakov K I et al. *Appl. Sci.* **11** 10087 (2021)
76. Unikal'naya nauchnaya ustanovka "Kriointegral" — "Tekhnologicheskii i izmeritel'nyi kompleks dlya sozdaniya sverkhprovodnikovykh nanosistem na osnove novykh materialov" (Unique research installation "Cryointegral" — "Technological and measurement complex for the development of superconducting nanosystems based on new materials"), http://www.cplire.ru/rus/kriointegral/index.html; http://ckp-rf.ru/usu/352529/
77. Khan F V et al. *J. Commun. Technol. Electron.* **68** 1219 (2023); *Radiotekh. Elektron.* **68** 1003 (2023)
78. Koshelets V P et al. *Phys. Rev. B* **56** 5572 (1997)
79. Ermakov A B et al. *IEEE Trans. Appl. Supercond.* **11** 840 (2001)
80. Kalashnikov K V et al. *IEEE Trans. Appl. Supercond.* **28** 2400105 (2018)
81. Paramonov M E et al. *Appl. Sci.* **12** 8904 (2022)
82. Koshelets V P et al. *Appl. Phys. Lett.* **68** 1273 (1996)
83. Koshelets V P, Shitov S V *Supercond. Sci. Technol.* **13** R53 (2000)
84. Koshelets V P et al. *IEEE Trans. Appl. Supercond.* **15** 960 (2005)
85. de Lange G et al. *Supercond. Sci. Technol.* **23** 045016 (2010)
86. Koshelets V P et al. *IEEE Trans. Terahertz Sci. Technol.* **5** 687 (2015)
87. Kinev N V et al. *J. Appl. Phys.* **125** 151603 (2019)
88. Kinev N V et al. *J. Commun. Technol. Electron.* **64** 1081 (2019); *Radiotekh. Elektron.* **64** 970 (2019)
89. Kinev N V et al. *IEEE Trans. Terahertz Sci. Technol.* **9** 557 (2019)
90. Kinev N V et al. *Phys. Solid State* **62** 1543 (2020); *Fiz. Tverd. Tela* **62** 1379 (2020)
91. Kinev N V et al. *Sensors* **20** 7267 (2020)
92. Hamilton C A, Shapiro S *Phys. Rev. B* **2** 4494 (1970)
93. Kinev N V et al. *IEEE Trans. Appl. Supercond.* **32** 1500206 (2022)
94. Kinev N V et al. *Radiophys. Quantum Electron.* **65** 593 (2023); *Izv. Vyssh. Uchebn. Zaved. Radiofiz.* **65** 651 (2022)
95. Sullivan D B et al. *J. Appl. Phys.* **41** 4865 (1970)
96. Likes R S, Falco C M *J. Appl. Phys.* **48** 5370 (1977)
97. Zimmerman J E, Silver A H *Phys. Rev. Lett.* **19** 14 (1967)
98. Kittara P, Withington S, Yassin G *J. Appl. Phys.* **101** 024508 (2007)
99. Kinev N V et al. *Phys. Solid State* **63** 1414 (2021); *Fiz. Tverd. Tela* **63** 1204 (2021)
100. Skalare A *Int. J. Infrared Millimeter Waves* **10** 1339 (1989)
101. Khan F V et al. *J. Commun. Technol. Electron.* **68** 983 (2023); *Radiotekh. Elektron.* **68** 897 (2023)
102. Koshelets V P et al. *IEEE Trans. Appl. Supercond.* **9** 4133 (1999)